Pure optical dephasing dynamics in semiconducting single-walled carbon nanotubes

ARTICLE *in* THE JOURNAL OF CHEMICAL PHYSICS · JANUARY 2011

Impact Factor: 2.95 · DOI: 10.1063/1.3530582 · Source: PubMed

5 AUTHORS, INCLUDING:

Alexander Green
Harvard University
66 PUBLICATIONS **3,896** CITATIONS

SEE PROFILE

Pure optical dephasing dynamics in semiconducting single-walled carbon nanotubes

Matthew W. Graham,[1] Ying-Zhong Ma,[1,2] Alexander A. Green,[3] Mark C. Hersam,[3] and Graham R. Fleming[1,a)]

[1]*Department of Chemistry, University of California, Berkeley, and Physical Biosciences Division, Lawrence Berkeley National Laboratory, Berkeley, California 94720, USA*
[2]*Chemical Sciences Division, Oak Ridge National Laboratory, Oak Ridge, Tennessee 37831, USA*
[3]*Department of Materials Science and Engineering and Department of Chemistry, Northwestern University, Evanston, Illinois 60208, USA*

(Received 24 August 2010; accepted 29 November 2010; published online 19 January 2011)

We report a detailed study of ultrafast exciton dephasing processes in semiconducting single-walled carbon nanotubes employing a sample highly enriched in a single tube species, the (6,5) tube. Systematic measurements of femtosecond pump–probe, two-pulse photon echo, and three-pulse photon echo peak shift over a broad range of excitation intensities and lattice temperature (from 4.4 to 292 K) enable us to quantify the timescales of pure optical dephasing (T_2^*), along with exciton–exciton and exciton–phonon scattering, environmental effects as well as spectral diffusion. While the exciton dephasing time (T_2) increases from 205 fs at room temperature to 320 fs at 70 K, we found that further decrease of the lattice temperature leads to a shortening of the T_2 times. This complex temperature dependence was found to arise from an enhanced relaxation of exciton population at lattice temperatures below 80 K. By quantitatively accounting the contribution from the population relaxation, the corresponding pure optical dephasing times increase monotonically from 225 fs at room temperature to 508 fs at 4.4 K. We further found that below 180 K, the pure dephasing rate ($1/T_2^*$) scales linearly with temperature with a slope of 6.7 ± 0.6 μeV/K, which suggests dephasing arising from one-phonon scattering (i.e., acoustic phonons). In view of the large dynamic disorder of the surrounding environment, the origin of the long room temperature pure dephasing time is proposed to result from reduced strength of exciton–phonon coupling by motional narrowing over nuclear fluctuations. This consideration further suggests the occurrence of remarkable initial exciton delocalization and makes nanotubes ideal to study many-body effects in spatially confined systems. © *2011 American Institute of Physics*. [doi:10.1063/1.3530582]

I. INTRODUCTION

Semiconducting single-walled carbon nanotubes (SWNTs) are one of the most intriguing nanomaterials due to their large aspect ratios, size tunable properties, and dominant many-body interactions.[1,2] While the SWNT electrical and mechanical properties have been well studied, the fundamental optical properties are continuously emerging as new synthetic and purification techniques are developed. Such optical characterization has fueled recent developments such as efficient *in vivo* photoluminescence imaging in live mice and demonstration of highly efficient carbon nanotube photodiodes.[3,4] The photophysical properties of this quasi-one-dimensional nanomaterial are determined by strongly bound Mott–Wannier type excitons, which arise from an electron–hole Coulombic interaction that is greatly enhanced from one-dimensional (1D) confinement effects.[5–7] Since the corresponding exciton binding energy composes a large fraction of the overall band-gap (~30% for (6,5) SWNTs), excitonic transitons completely determine the optical properties of semiconducting SWNTs. As a consequence, the linear abosorption and photoluminesence spectra produce relatively sharp peaks from transitions from bound exciton states [see, Fig. 1(a)]. *Ab initio* calculations show that each such transition (denoted E_{11}, E_{22}, and so on) occurs within a manifold of both the optically bright and dark states, the latter of which are believed to play a critical role in exciton population relaxation processes[8,9] and in determining the overall photoluminescence yield.[10,11]

The excitons initially possess a definite phase relationship among themselves and with the electromagnetic radiation creating them.[12] As such, the coherently created excitons can be spatially delocalized on an extended scale limited in principle only by the wavelength of the laser light. For semiconducting SWNTs with a length scale of ~1 μm or shorter, this would suggest that E_{11} excitons may be initially delocalized up to the length of the nanotube. Currently, reported estimates for the exciton delocalization lengths vary greatly from tens to hundreds of nm and will depend critically on the timescale of the measurement.[10,13] Subsequent scattering with phonons, defects, and impurities, etc. will lead to an exponential loss of coherence within an ensemble of SWNTs and eventually exciton localization to a finite spatial length equal to its inherent radius of ~1–2 nm.[5] A quantitative measure of this timescale where exciton coherence persists is

a)Author to whom correspondence should be addressed. Electronic mail: grfleming@lbl.gov.

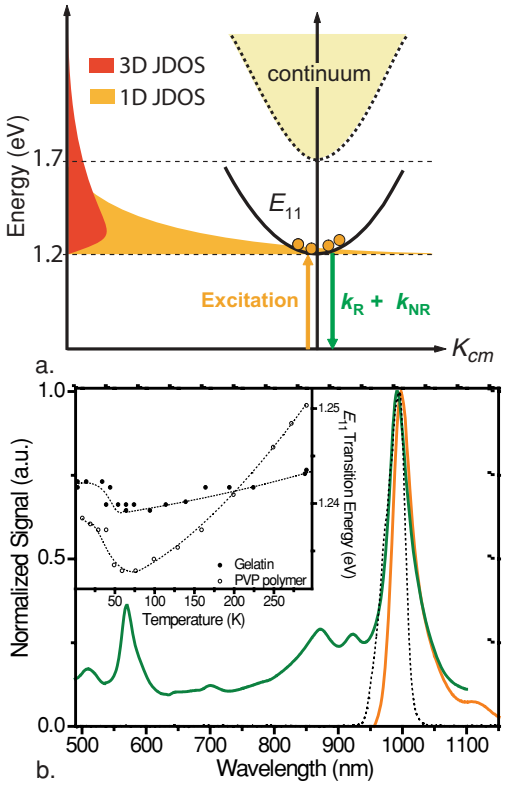

FIG. 1. (a) Simplified electronic energy diagram for a semiconducting SWNT depicting the strongly bound E_{11} exciton state with respect to the continuum vs the quasiparticle center of mass (K_{cm}). The overlaying 1D joint density of states (JDOS) diverges near the band minimum, enabling simultaneous excitation of multiple excitons. Subsequent relaxation pathways can be both radiative (k_R) and nonradiative (k_{NR}) and may also involve a low-lying state (not shown). (b) E_{11} linear absorption (green line) and steady-state fluorescence emission (orange line) spectra of (6,5) tube embedded in PVP polymer, together with the spectrum of the 45 fs laser pulse (dotted line). The inset shows the energies of the absorption maxima plotted as a function of temperature for two polymer–SWNT composite films prepared using gelatin (filled circles) and PVP (open circles) polymers, respectively.

the dephasing time (T_2), and its determination also provides a time-domain measurement of the homogeneous linewidth through the inverse proportionality, $\Gamma_h = 2\hbar/T_2$.[14] During the dephasing time both population and the ensemble phase will decay; however, the remaining excitons may be extensively delocalized along the tube.

The homogeneous linewidths of SWNT ensembles were first measured by femtosecond three-pulse photon echo peak shift (3PEPS) spectroscopy, which provided an indirect estimation of the T_2 timescales.[15] Shortly after, direct determination of the dephasing timescales was preformed using a femtosecond two-pulse photon echo (2PE) technique on a sample highly enriched in the (6,5) tube species. Using 2PE, long-lived E_{11} coherences with a T_2 of 170 fs were reported at room temperature.[16] Similar dephasing times have been also reported for other tube types using indirect two-pulse photon echo peak shift measurements.[17] Observation of long electronic dephasing times at room temperature is striking in comparison to molecules, molecular complexes, and aggregates which typically dephase on a sub 10 fs timescale.[18,19] Crystalline systems such as two-dimensional GaAs quantum wells have moderately longer dephasing times approaching ~95 fs at 294 K.[12,20,21] Additionally, previous measurements at different excitation intensities and lattice temperatures (77–292 K) showed that both exciton–exciton and exciton–phonon scattering profoundly influence the dephasing timescales and the homogeneous linewidths of the E_{11} transition.[16,17]

Together, the 3PEPS and 2PE results independently show that the homogeneous linewidth associated with the (6,5) E_{11} transition is at least fourfold smaller than the inhomogeneous contributions.[15,16] Similar homogeneous linewidths have been also obtained from frequency-domain single-tube measurements.[22–24] One advantage of the ensemble based approach using photon echo spectroscopy is that its inherent averaging accounts for the differences among individually separated tube (length, defects, etc.) and local environmental disorder. While correspondence can be found between the results obtained from time-domain ensemble measurements and frequency-domain single-tube spectroscopy, direct comparison is hampered by the often highly variable linewidths obtained from single-tube measurements even for the tubes with same chirality. In addition, all reported single-tube fluorescence experiments employ indirect excitation of the E_{11} band through its corresponding E_{22} manifold, vibronic bands or off-resonance. The ensuing relaxation to the radiative E_{11} state is typically accompanied by multiphonon emission, which can cause additional dephasing not present in time-domain photon echo measurements employing direct E_{11} excitation.[25]

Although both time-domain photon echo and frequency-domain single-tube approaches are powerful tools to quantify the dephasing times (T_2), neither of them can directly provide the pure dephasing time (T_2^*), which is related to the dephasing time T_2 and the population lifetime (T_1) through the following well-known relation:

$$\frac{1}{T_2} = \frac{1}{2T_1} + \frac{1}{T_2^*}. \tag{1}$$

While the T_2 timescales can be readily obtained from 2PE measurements, proper determination of the T_1 values is not straightforward owing to the general existence of complicated multiexponential decays in SWNTs. The shortest component of the population relaxation can approach the typical T_2 times,[2] and in this case a substantial contribution to spectral linewidth from the population lifetime broadening is expected. Hence, simultaneous measurement of both population and exciton dephasing timescales are crucial to elucidate the pure dephasing timescale (T_2^*) for E_{11} exciton decoherence from exciton–phonon scattering.

In this contribution, we employ complimentary femtosecond spectroscopic techniques including pump–probe, 2PE, and 3PEPS spectroscopy to determine pure optical dephasing times associated with the E_{11} transition. Our experiments were conducted across a broad temperature range (2.5–292 K) and at various excitation intensities and on samples highly enriched in the (6,5) tube type dispersed individually either in aqueous solution or polymer composite films. Analysis of the resulting data further permitted us to distinguish specific contributions to homogeneous linewidth from longitudinal optical and acoustic phonons and to observe an intrinsically large

linewidth in the low temperatures limit given by the environmental disorder. Preceding the experimental methods, this paper is organized as follows: the 2PE results are presented and T_2 is extracted as function of temperature and excitation fluence (Sec. III A), next the population broadening contribution ($1/T_1$) are determined and modeled (Sec. III B), the resulting pure dephasing rates ($1/T_2^*$) are calculated and the overall line broadening mechanisms discussed (Sec. III C). Next, 3PEPS results are compared against 2PE measurements (Sec. III D), the role of local environments on dephasing rate is examined (Sec. III E), and lastly the role of exciton delocalization on E_{11} dephasing dynamics is discussed (Sec. III F).

II. EXPERIMENTAL

Optical spectrocscopic investigations of SWNTs are often complicated by the existence of multiple structurally distinct tube species and by a variable amount of bundles being present. Central to all experiments reported in this paper is the use of a sample highly enriched in a single semiconducting tube species, the (6,5) tube. In combination with resonant probe of the E_{11} or E_{22} excitonic bands, this allows us to access the ultrafast dynamics associated with a single tube type. The sample was obtained using a density-gradient ultracentrifuguation procedure,[26] and the resulting aqueous suspensions of individualized SWNTs were mixed with water-soluble gelatin or polyvinylpryrolidone (PVP) polymer and then cast into thin (roughly 400 μm) polymer composite films. Use of such polymer films greatly suppressed laser light scattering arising from slow tube motions occurring in aqueous solution, and enabled measurements at sufficiently low excitation intensities with a good signal-to-noise ratio over a broad temperature range.

The linear absorption and steady-state fluorescence emission spectra measured for SWNTs embedded in a PVP film at room temperature are shown in Fig. 1(b). Upon excitation of the E_{22} transition at 572 nm, similar relative fluorescence yields are obtained compared with the starting aqueous samples. Additionally, the absence of a broad, intense emission in the 1150 nm spectral region indicates that the tube bundling is insignificant.[27,28] Measurements at low temperatures were carried out by placing the SWNT–polymer composite films in direct contact with a Janis ST-100 cold finger which operates under continuous liquid helium flow. The sample temperature was continuously controlled by interfacing the cryostat with a Lakeshore 331S temperature controller. To ensure high optical quality and resonant excitation of the (6,5) tubes at all measured temperatures, linear absorption spectra were recorded from 4.4 to 292 K, and the resulting E_{11} peak positions are shown in Fig. 1(b) (inset). Upon cooling, the PVP composite films showed a maximum 5 nm redshift, which may be attributed to hydrostatic tube strain effects.[29,30] In contrast, gelatin films yielded a comparatively small redshift (maximum 2 nm), suggesting a somewhat weaker hydrostatic effect. Moreover, a small spectral blueshift was observed for both the films at temperature below ~80 K. Similar low temperature blueshifts have been previously reported experimentally and predicted theoretically for selected tube types.[31] In addition to the measurements conducted on these films, we also performed experiments using the aqueous solution at room temperature. In this case, a thin quartz cell of 100 μm pathlength was used, which helps to minimize the thermal lensing effects induced by laser beams.

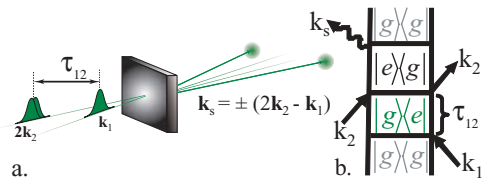

FIG. 2. (a) The laser beam geometry of the 2PE experiment with emerging echo signals. (b) A double-sided Feynman diagram shows the temporal state evolution, laser pulse $\mathbf{k}_1$ prepares a coherent superposition ($|g\rangle\langle e|$) between ground and the E_{11} excited state, which subsequently dephases over time τ_{12}. The detected 2PE scattering signal ($\mathbf{k}_s$) is stimulated by the remaining two interactions ($\mathbf{k}_2$).

The experimental setups for femtosecond 2PE, 3PEPS, and pump–probe spectroscopy have been described in detail previously and only a brief account will be given here.[12,14,32] The light source was an optical parametric amplifier pumped by a 250 kHz Ti:Sapphire regenerative amplifier, which produces 40–65 fs laser pulses tunable in the visible and near-infrared regions. A combination of a waveplate and a polarizer was used to control the intensity of laser pulse from 0.3 to 15 μJ/cm^2 for all experiments described in this paper.

The 2PE experiments were performed by directly exciting the E_{11} state of the (6,5) tube with 45 fs laser pulses centered at 998 nm for the SWNT–gelatin film, 995 nm for the SWNT–PVP film [see Fig. 1(b) for the laser pulse spectrum], and 990 nm for aqueous solution sample. Additional experiments were also performed at 1012 nm to excite the red-edge of the E_{11} absorption band for the PVP–SWNT films. In these experiments, two nearly equal intensity laser pulses were focused to a spot of 148 μm diameter. The first pulse with wavevector $\mathbf{k}_1$ creates a coherent macroscopic polarization of the exciton ensemble that is allowed to dephase over a variable delay time or coherence time (τ_{12}). After time τ_{12} has elapsed, a second pulse $\mathbf{k}_2$ arrives producing an interference grating with respect to the partially dephased coherent polarization created by $\mathbf{k}_1$. This transient grating diffracts incident photons into phased-matched direction $2\mathbf{k}_2$-$\mathbf{k}_1$ as shown in Fig. 2, which is detected in a time-integrated manner with an InGaAs photodiode and a lock-in amplifier. A measurement of the diffracted signal as function of positive τ_{12} delays gives a nearly monoexponential decay, and the corresponding timescale (τ_{decay}) can be accurately extracted through a least squares deconvolution fitting algorithm with explicit consideration of finite pulse duration. For strongly inhomogeneously broadened systems such as semiconducting SWNTs,[15] the dephasing time T_2 can be obtained directly from the following relation $T_2 = 4\tau_{\text{decay}}$.[33]

The dynamics of exciton population relaxation was monitored by femtosecond pump–probe spectroscopy. Upon excitation of the E_{22} transition with 48 fs laser pulses centered at 570 nm and subsequent rapid interband relaxation,[34] the dynamics of the resulting E_{11} excitons is probed selectively at chosen wavelengths with a white-light continuum. The

detection unit consists of a single-grating monochromator, an InGaAs photodiode and a lock-in amplifier. The polarization of the pump beam was set to the magic angle (54.7°) with respect to probe beam, which enables us to eliminate potential contributions from tube orientation. The measurements were performed at several sample temperatures which was chosen to be same as used for our 2PE experiments. A least squares deconvolution algorithm was applied to extract the timescales of the decay kinetics employing a model function that consists of sum of multiple exponents.

To investigate both optical dephasing and spectral diffusion processes, 3PEPS was used as an extension of the 2PE approach where the laser pulse was instead divided into three replicas ($\mathbf{k}_1, \mathbf{k}_2, \mathbf{k}_3$).[35] The details of this technique and its application to SWNTs at room temperature has been previously described.[15,33] Briefly, the 3PEPS signal were simultaneously detected in two phase-matching directions ($\mathbf{k}_1 - \mathbf{k}_2 + \mathbf{k}_3$ and $-\mathbf{k}_1 + \mathbf{k}_2 + \mathbf{k}_3$) as a function of coherence time (τ_{12}) and an additional delay between pulses 2 and 3, the population time (t_{23}). At a given population time, two photon echo profiles were measured and the corresponding peak-shift (τ^*) is defined as half of the temporal offset of the two signal maxima. A plot of the peak shift τ^* as a function of population time allowed us to examine both optical dephasing (for $t_{23} = 0$) and spectral diffusion processes ($t_{23} > 0$) for temperatures ranging from 4.4 to 292 K.

III. RESULTS AND DISCUSSION

A. Exciton–exciton scattering dynamics

The large absorption cross-section of semiconducting SWNTs facilitates the creation of multiple excitons per tube, which will experience enhanced mutual interactions because of one-dimensional confinement.[2] A quantitative estimate for the number of excitons created can be obtained using an absorption cross-section ($\sim 1 \times 10^{-17}$ cm^2 per SWNT carbon atom),[36] the mean tube length of 600 nm for our samples,[26] a measured beam waist (148 μm), and the total incident excitation intensity used. The excitation intensity was varied over fiftyfold corresponding to a mean exciton population of 0.8–42 per tube or alternatively an exciton density (N_x) ranging from 1.3 to 70 ($\times 10^4$) cm^{-1}. One consequence of populating many excitons in a spatially confined region is a significant enhancement in exciton–exciton scattering events along the nanotube axis.[25] Previous work has shown that such exciton–exciton scattering and annihilation contributes significantly to optical dephasing in SWNTs.[37]

Figures 3(a) and 3(b) show the 2PE data measured for different excitation fluences at 4.4 and 292 K, respectively (semilog scale plotted). At all temperatures, the decay follows monoexponential behavior very closely. The 2PE profile decays markedly faster with increasing excitation fluence, providing direct evidence for dephasing induced by exciton–exciton scattering. While a similar intensity dependence has been recently reported,[16,17] the results obtained here are reported down to temperatures as low as 2.5 K and extract the optical dephasing rate directly from the echo decay profile. As has been recently reported,[25,38] the exciton dephasing rate ($1/T_2$) or equivalently, the homogeneous linewidth, contains contributions from line broadening induced by both inelastic exciton–phonon ($\Gamma_{\text{ex-ph}}(T)$) and exciton–exciton scattering ($\Gamma_{\text{ex-ex}}(N_x, T)$).[15,17,37] These contributions sum to give the overall effective homogeneous linewidth,

$$\Gamma_h(N_x, T) = \Gamma_0 + \Gamma_{\text{ex-ex}}(T)N_x + \Gamma_{\text{ex-ph}}(T), \qquad (2)$$

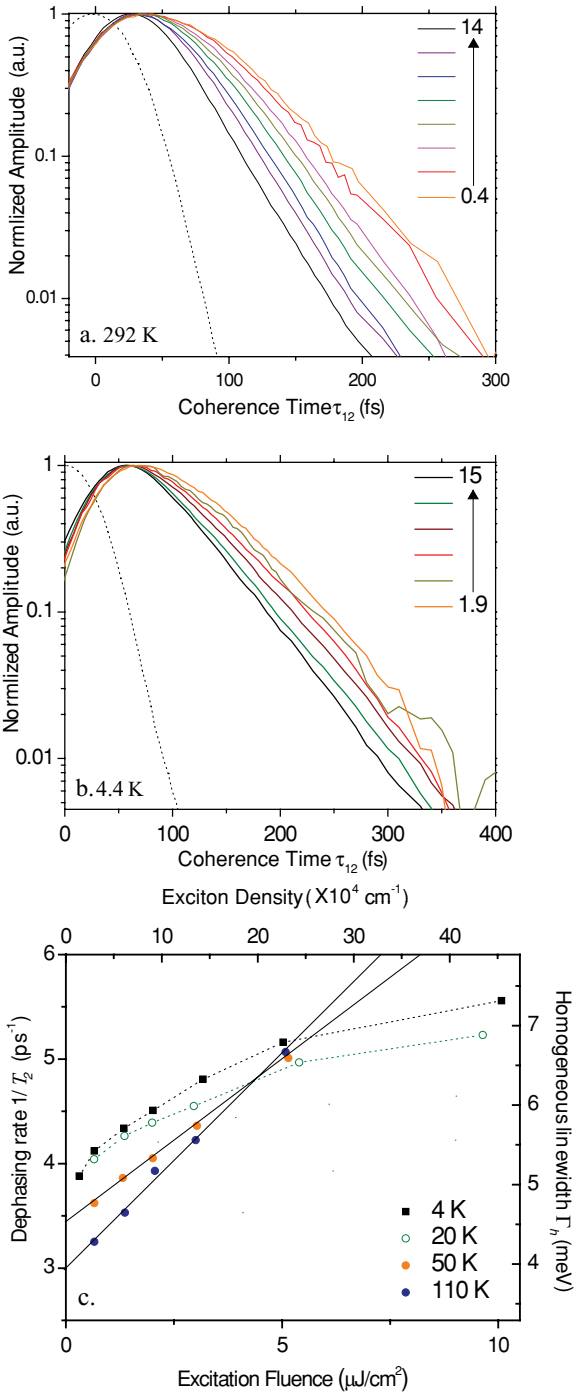

FIG. 3. 2PE decays profile showing the excitation intensity dependence for the (6,5) SWNT collected at (a) 292 K in aqueous solution and (b) 4.4 K in PVP polymer under various excitation fluences as indicated in the plots (in μJ/cm^2) (c) Plot of the extracted dephasing rate, $1/T_2$, as a function of excitation fluence shown at four different temperatures. Plots can be extrapolated to the zero-intensity limit where contributions from exciton–exciton scattering are negligible.

where Γ_0 is the intrinsic linewidth at $T = 0$ K.[38] As exciton density is increased, the exponential decay rate of the 2PE signal increases by one fold across all temperatures measured (see, Fig. 3, note the semilog intensity scale). Other spatially confined systems such as quantum wires[39] and CdSe quantum dots[40] also exhibit clear signatures of intensity induced dephasing. A substantial Γ_{ex-ex} contribution to the linewidth is consistent with exciton confinement effects leading to enhanced exciton–exciton scattering. Carbon nanotubes in particular are not only strongly confined 1D systems, but have large absorption cross-sections ($\sim 5.5 \times 10^{-13}$ cm^2 for a 600 nm (6,5) tube), making them an ideal systems to observe such intensity dependent contributions to the exciton dephasing rate.

In order to reach a limit where scattering from multiexciton interactions (i.e., Γ_{ex-ex}) can be safely neglected, the beam fluence was incrementally lowered, permitting extrapolation to the zero intensity limit [see Fig. 3(c)]. The resulting intensity-independent dephasing rate (or intrinsic homogeneous linewidth) is then obtained. For the majority of temperatures measured the dephasing rate varied linearly with the exciton density (N_x) according to Eq. (2). Below approximately 30 K and above 200 K however, the dephasing rates obtained have significant curvature with excitation intensity, suggesting that the exciton–exciton (Γ_{ex-ex}) and exciton–phonon (Γ_{ex-ph}) dephasing contributions may be coupled. In these cases, a polynomial expression was used to extrapolate to the zero intensity limit. The results obtained are in good accord with measurements published earlier reporting the intensity-dependent exciton dephasing rate down to 77 K.[16] Detailed studies examining the contributions from exciton–exciton scattering to optical dephasing can be found elsewhere.[25,37] In the following sections we instead focus on the extrapolated results in the zero intensity limit, which effectively eliminates the contribution from the Γ_{ex-ex} term to the homogeneous linewidth.

B. Temperature-dependent contributions from E_{11} population relaxation

Pure optical dephasing times are often considered to be identical to the T_2 time obtained directly from 2PE experiments, and the contributions from population relaxation are neglected by assuming that its lifetime is significantly long (i.e., $1/2T_1 \ll 1/T_2$). The population relaxation detected for the (6,5) nanotubes by pump–probe experiments however, contains a dominant decay component with a timescale similar to the T_2 time. This means that explicit account of the population decay time (T_1) is crucial to correctly obtain the pure optical dephasing time T_2^*.

To account for the contributions from population decay, we performed pump–probe measurements for the (6,5) tubes embedded in both PVP polymer and gelatin composites at different temperatures [see Fig. 4(a)]. For the PVP composites, the same temperatures were chosen as used for our 2PE measurements. Extraction of the decay timescales from the pump–probe data involves use of a least-squares deconvolution algorithm and a model function consisting of multiexponential components. We obtained satisfactory fits for a majority of

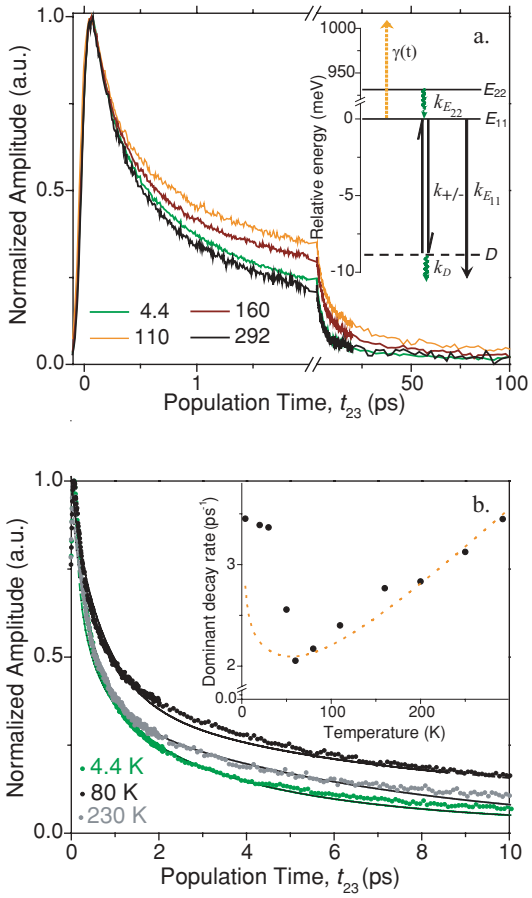

FIG. 4. (a) Pump–probe data collected for the (6,5) tube embedded in PVP polymer matrix at four different temperatures (in K). The experiments were performed by exciting the E_{22} transition at 570 nm, and probing the E_{11} state at 998 nm. All the data were normalized at peak amplitudes of the pump–probe signals, and the resulting decay profile appears largely independent of the pump fluence. The inset shows the three-state model used to model the experimental data, which includes a radiative decay pathway from the E_{11} state to the ground-state with a rate constant $k_{E_{11}}$, and all others are nonradiative pathways. (b) Simulated decay kinetics (solid lines) for chosen temperatures. The inset shows the temperature dependence of the extracted population decay rates (black circles) for the fastest (and dominant) decay component obtained from a multiexponential fit. The dotted line (orange) show the simulated results.

our data with a model function of three exponents, but for those measured near room temperature ($T \geq 250$ K), an additional exponential component was needed. Among these three or four components, the fastest decay component is always dominant and has an approximate relative weight of 60% of the total amplitude. The extracted lifetime for this fastest lifetime component ranged from 290 to 460 fs as the temperature was lowered from 292 to 80 K. The lifetime associated with the second decay component ranged from 2.7 to 5.6 ps over the same temperature range with a relative amplitude of 30%, and the slowest decay component has a lifetime of 140 ps with about 10% relative amplitude. It is clear from Eq. (1), that the two slower decay components will not contribute appreciably to the pure dephasing rate. Also, their significantly smaller amplitudes in combination with their relatively weak temperature dependence further reduce their influence on the obtained pure dephasing times T_2^*. Thus, we will instead

focus primarily on modelling the initial, fast decay portion of the pump–probe data collected at various temperatures.

The inset in Fig. 4(b) shows the dominant population decay rates extracted from the fastest exponential relaxation component at each temperature measured. Upon cooling the sample from 292 to 80 K, a roughly linear dependence of the population decay rate on temperature is found. Such a rate increase with temperature is normally expected for systems dominated by nonradiative decay primarily mediated by exciton–phonon scattering.[41] Below the 80 K threshold, a marked increase in the E_{11} population decay rate is observed, which can be seen from the kinetics shown in Fig. 4(a). To model such an acceleration in the initial decay component for (6,5) SWNTs, we adopted a phenomenological three-state model previously used to describe temperature dependence of steady-state and time-resolved fluorescence kinetics of semiconducting SWNTs.[10,42,43] This three-state model allows for rapid thermalization of the optically bright E_{11} state with a third low-lying state [labeled D, see the energy level diagram in the inset of Fig. 4(a)]. At sufficiently low temperatures, the acoustic phonon modes mediating the $E_{11} \leftrightarrow D$ thermalization are no longer excited, which will effectively halt the uphill energy transfer from D to E_{11}. This consideration indicates that an enhancement in the exciton population decay will occur when the temperature reaches a certain range, which is in line with the shortened lifetime associated with the fastest decay of the fastest decay component observed below 80 K [see, Figs. 4(a) and 4(b)].

To quantitatively simulate the population relaxation dynamics, we begin with the following coupled differential equations:

$$\frac{dn_{E_{11}}}{dt} = k_{E_{22}} n_{E_{22}} - (k_{E_{11}} + k_-) n_{E_{11}} + k_+ n_D - \frac{1}{2}\gamma_0 t^{-1/2} n_{E_{11}}^2, \tag{3}$$

$$\frac{dn_D}{dt} = -(k_D + k_+) n_D + k_- n_{E_{11}}, \tag{4}$$

where $n_{E_{11}}$ and n_D represent the exciton populations at the E_{11} and D states, respectively, and the k parameter describes the rate constants for population relaxation shown in the inset of Fig. 4(a). Since, the $E_{22} \rightarrow E_{11}$ relaxation is known to be fast (roughly 50 fs) (Ref. 34) compared to our pulse duration, we can assume that the E_{11} band is impulsively excited (i.e., $k_{E_{22}} = 0$). A significant addition in our model from that reported previously is that we explicitly take an exciton–exciton annihilation pathway into account. Consequently, an additional relaxation pathway originated from the E_{11} state is included in Eq. (3). We further assume that the corresponding annihilation rate can be described by $\gamma(t) = \gamma_0 t^{-(1-d/2)}$ with the dimensionality parameter d being equal to 1 and γ_0 being time-independent and therefore describe diffusion-limited exciton annihilation.[41,44] Using Eqs. (3) and (4) to solve for $n_{E_{11}}(t)$ we were able to reproduce approximately the temperature dependence of the decay rates shown in Fig. 4(b) (inset).

In order to explicitly include the temperature dependence, a phonon assisted scattering process between the E_{11} and the low-lying state D is included. For the above simulation, we assumed that the E_{11} exciton band is parabolic, along with a radiative decay ($k_{E_{11}}$) from the optically bright E_{11} state and nonradiative relaxation (k_{NR}) from the D state to ground-state. The radiative relaxation can occur only from excitons located within a small region with an energy $\Delta \cong 0.37$ μeV above the band minimum, which is accessible by a photon's momentum.[9,43] According to Spataru *et al.*,[45] for an infinite length tube the E_{11} radiative decay rate can be approximated outside the $T \rightarrow 0$ region as

$$k_{E_{11}} = k^{\circ} \sqrt{\frac{\Delta}{k_b T}}, \tag{5}$$

where k° is a radiative decay parameter (at $K_{\mathrm{cm}} = 0$) and k_b is the Boltzmann constant. A corresponding intrinsic radiative lifetime of 2.5 ps was used. The actual effective radiative lifetime measured (i.e., $k_{E_{11}}$) is orders of magnitude larger at all temperatures because of the exciton momentum distribution and potential thermalization with the low-lying state, D. This lifetime value is somewhat shorter than the ~10 ps predicted for the (8,0) tube type by *ab initio* calculations.[45] For temperatures above ~80 K, the E_{11} state is thermally accessible for the excitons situated at the state D and the corresponding uphill and downhill rates (k_+ and k_-) can be approximately related by detailed balance as follows:

$$k_+ = k_- \exp\left(\frac{-\Delta E_D}{k_b T}\right), \tag{6}$$

where ΔE_D is the energy difference between the two states. This energy difference is found to be approximately 9 meV and is consistent with results (5–8 meV) obtained from magnetophotoluminescence spectroscopy.[11] The potential involvement of this low-lying state D has been shown to further increase the effective radiative lifetime, particularly in $T <$ ~80 K region in time-resolved photoluminescence work.[43,46]

Both the the downhill relaxation (k_-) and the subsequent decay from the low-lying D state (k_D) are assumed to be nonradiative, and their associated temperature dependence can be approximated as[47,48]

$$k_{\mathrm{NR}} = k_c + C \exp\left(\frac{-\theta_k}{k_b T}\right), \tag{7}$$

where k_c, C, and θ_k are fitted parameters, which are determined to be 0.06 , 0.6 , and 90 K for the k_- rate. For relaxation from the D state, we obtain a value of $k_D = 0.15$ ps^{-1} for our simulations with no temperature dependence required for our temperature range. If we assume that the exciton annihilation rate is largely temperature independent we can set $\gamma_0 = 0$ to get the initial rate dependence on temperature; our analysis then follows the one presented by Scholes *et al.* applied to temperature dependent photoluminescence rates.[43] Using the fitted parameters to compute the initial decay rate, the three-state model reproduces the temperature-dependent trend observed for the dominant E_{11} kinetic relaxation rate [see Fig. 4(b), inset].

The above model (with $\gamma_0 = 0$) gives a biexponential decay for E_{11} kinetics, whereas at least three exponential decay components were required to numerically approximate our pump–probe measurements. Inclusion of exciton–exciton

annihilation introduces a nonexponential component which allows us to roughly model the temperature-dependent kinetic decay. Using γ_0 values ranging from 0.4 to 1.6 $ps^{-1/2}$, we solved the differential system of Eqs. (3) and (4) numerically for temperatures ranging from 4 to 290 K. At most temperatures, the resulting simulated decay curves (solid lines) could reproduce the experimental decay well [see Fig. 4(b)]. Full treatment however would require explicit consideration of the delayed ground state recovery contribution from n_D. Since the cross-sectional prefactors are not well-known, we instead assumed that the population occupying $n_D(t)$ is small compared to the E_{11} and ground state population. A more complete treatment of the temperature dependent kinetics may be reported in future works.

The involvement of low-lying states such as the phenomenological D state described here, has also been applied to model the temperature dependence of SWNT fluorescence quantum yields. The precipitous decrease in the quantum yield observed below 80 K suggests that any radiative decay out of the low-lying states must be comparatively small,[42,46,49] which is supported by a significant decrease of radiative rate.[46] In many works, low-lying states such as the D state has been commonly ascribed to the $1g$ state originally proposed from calculations using a 1D hydrogenic model exciton wavefunction.[5,43] The $1g$ state is expected to be optically dark from parity selection rules for a one-dimensional SWNT.[10] However for intra-excitonic transitions from the optically bright E_{11} $1u$ state to $1g$, rapid scattering and thermalization between states of different parity is allowed.[49–51]

Previous pump–probe measurements at temperatures between 77 and 293 K showed that the decay times increase roughly linearly with decreasing temperature.[52] A similar temperature dependence was also observed from time-resolved fluorescence measurements at both the single-tube and ensemble levels.[46,53] However, when the temperature is lower than 80 K a further decrease of the temperature appear to have little effect on the decay times. In contrast, in the pump–probe results reported here we observe an acceleration in initial decay rate for T < 80 K. One possible reason is the different time resolutions of the time-resolved fluorescence experiments and the pump–probe technique used here.

Modeling of the temperature dependent pump–probe decay curves, suggests that the low temperature rate acceleration is physically consistent with involvement of a low-lying state. While a similar temperature-dependent trend was also observed for (6,5) SWNTs in a gelatin composite environment (data not shown), we nonetheless cannot completely rule out unforeseen environmental considerations as an alternate explanation. Regardless of the precise physical origin of the observed acceleration in E_{11} population decay rate at low temperatures, we can use the dominant initial decay rates plotted in Fig. 4(b) (inset) to effectively remove the contributions of population relaxation from our 2PE results, allowing us to determine T_2^* directly.

C. Pure optical dephasing timescales

Semiconducting SWNTs have been characterized by weak exciton–phonon coupling, an observation consistent

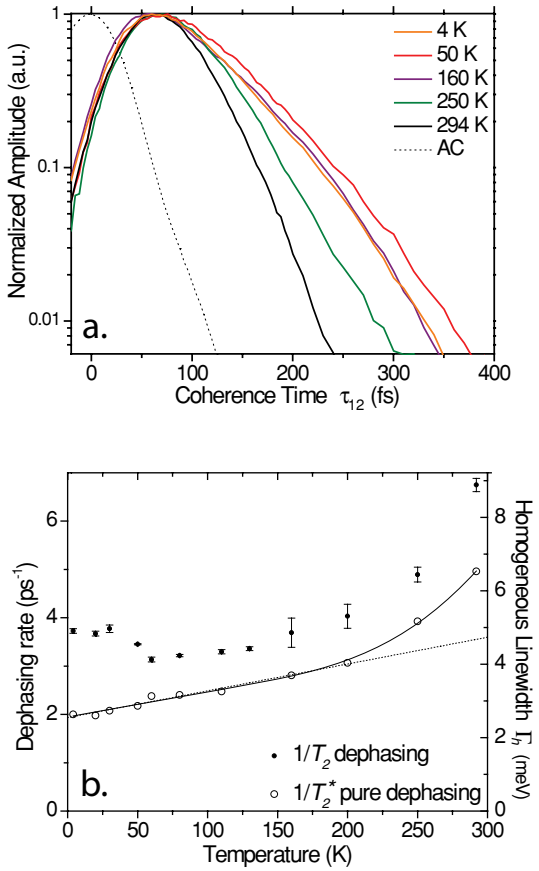

FIG. 5. (a) 2PE signals collected for the (6,5) tubes embedded in a PVP polymer film at different temperatures. A total excitation fluence of 6.0 $\mu J/cm^2$ was used for the measurements. (b) Plot of dephasing rates ($1/T_2$) and pure dephaing rates ($1/T_2^*$) vs temperature, which has a predominately linear slope (dotted line) consistent with optical dephasing from one-phonon processes. The solid line is a fit to the line-broadening function given in Eq. (8).

with both the small Stokes shift (e.g., ~4 nm in Fig. 1(a)) and *ab initio* calculations.[54] In accord, a 205 fs dephasing time is extracted for (6,5) SWNTs in aqueous solution at 292 K [see Fig. 3(a), low intensity limit]. Such long dephasing times at room temperature are indicative of weak exciton–phonon coupling strength. To better understand the physical origin of this weak coupling, 2PE traces were measured as a function of excitation fluence at fixed temperature increments down to 2.5 K. Consistent with previous T_2 times reported down to 77 K,[16] the extracted dephasing times increase only moderately (to 320 fs) upon cooling to 80 K. Extending the experiment to lower temperatures revealed an unexpected marked increase in the 2PE decay rate [see Fig. 5(a) and 5(b)]. Since lowering temperature necessarily decreases the phonon population, the observed increase in dephasing rate for T $\lesssim$ 80 K plotted in Fig. 5(b) is not consistent with line-broadening associated with exciton–phonon interactions (i.e., $\Gamma_{ex-ph}(T)$).

For all temperatures examined, we find the population dynamics are sufficiently fast to significantly broaden the corresponding homogeneous linewidths. Using Eq. (1), the contributions from population relaxation (T_1) are removed and the pure dephasing rate ($1/T_2^*$) is calculated. The $1/T_2^*$ rate is plotted in Fig. 5(b) (open circles) and has a distinctly different temperature dependence than the $1/T_2$ rate owing to an

acceleration in the initial E_{11} population decay rate ($1/T_1$) for T $\lesssim$ 80 K. In particular, the pure dephasing rate increases linearly in $T \lesssim 180$ K region. Such a linear rate dependence on temperature is a strong indicator of optical dephasing induced by one-phonon interactions.[12]

To fit the pure dephasing rates obtained, the following line-broadening function is used to determine what exciton–phonon scattering processes contribute to optical dephasing of the E_{11} excitation for (6,5) SWNTs,

$$\Gamma_h(T) = \Gamma_0 + aT + \frac{b}{e^{(\hbar\omega_{LO}/k_bT)} - 1}, \tag{8}$$

which is shown in Fig. 5(b) as the fitted solid line.[12] The first term Γ_0, represents the finite homogeneous linewidth at $T = 0$ K, which is 2.45 $\pm$ 0.05 meV (or $T_2^* \cong 535$ fs). The second parameter is the linear temperature-dependent line-broadening rate $a = 6.7 \pm 0.6$ μev/K and corresponds to one-phonon scattering processes commonly from acoustic phonons. For T $\lesssim$ 180 K, we find such one-phonon acoustic scattering processes are the dominant contribution inducing pure optical dephasing [shown by dotted linear fit in Fig. 5(b)]. Remarkably similar linear line-broadening rates have also been reported for GaAs quantum wells derived from similar 2PE analysis.[20,21] The last term in Eq. (8), provides contributions from optical phonon scattering which scales with the Bose optical phonon occupation factor. The corresponding fit suggests an intrinsic optical phonon energy of $\hbar\omega = 1028 \pm 231$ cm^{-1} with $b = 250 \pm 180$ meV. However, the sparsity of points collected in this T > 180 K region previously investigated in detail by Ma *et al.*,[16] prevents accurate assignment of the optical modes involved. Nonetheless, within the error calculated, the previously implicated traverse optical (TO) mode at 860 cm^{-1},[16] or the longitudinal acoustic + TO mode present at 960 cm^{-1} are potential candidates.[55]

Reasonable correspondence is found between our time-domain study on an ensemble of (6,5) SWNTs and recently reported single nanotube photoluminescence work on (9,8) tubes. Single-tube measurements reported a nearly identical low temperature linewidth of ~2.5 meV.[23] This particular single-tube measurement also produced a linewidth which scaled linearly with temperature (below ~160 K). The reported slope, however, was almost three times as steep as the values we extracted for (6,5) SWNTs.[23] A more meaningful comparison however would require information on the population lifetimes associated with the (9,8) SWNTs investigated in this single-nanotube study.

The observation of a significant homogeneous linewidth ($\Gamma_0 = 2.45$ meV) as $T \to 0$, suggests the presence of a large intrinsic environmental disorder that should be highly sample dependent. Calculations by Perebeinos *et al.* suggest that even a small amount of spectral diffusion from the surrounding environment can give rise to a significant homogeneous line-width as T $\to$ 0.[10] To investigate the the origin of this low-temperature disorder, the role of the local environment on dephasing processes will be examined in Sec. III E.

D. Spectral diffusion contribution: A 3PEPS measurement

The timescales extracted from 2PE ($T_2 = 205$ fs) and pump–probe decay ($T_1 = 372$ fs), suggest a room temperature pure dephasing time of 283 fs for aqueous (6,5) SWNTs. In order to investigate this apparently weak exciton–phonon coupling associated with the E_{11} state, we next examine the role of spectral diffusion processes for $t_{23} > 0$ by performing 3PEPS measurements at different temperatures. In 3PEPS, the photon echo signal is simultaneously collected in the $\mathbf{k}_1 - \mathbf{k}_2 + \mathbf{k}_3$ and $-\mathbf{k}_1 + \mathbf{k}_2 + \mathbf{k}_3$ phase matching directions, allowing access to the time delay between the second and third pulses corresponding to the population time (i.e., t_{23}). Here we briefly report the results of a temperature-dependent 3PEPS measurement; full details on the 3PEPS spectroscopy of semiconducting SWNTs at room temperature have been reported elsewhere.[15]

When the time delay $t_{23} = 0$, the 3PEPS (τ^*) experiment provides an indirect measurement optical dephasing time.[17] While there is no analytic relation between the peak shift and T_2, both quantities scale with the mean square of E_{11} state frequency fluctuations (Δ_m^2) that are modulated by the phonon bath.[33] After an established scaling ratio is used to correct for the pulse durations employed,[56] we find the numerically converted initial peak shift values agree with the corresponding dephasing rates obtained from 2PE experiments collected under the same excitation fluence [see Fig. 6(a)]. Such a non-monotonic computation of peak shift from T_2 has been applied previously to SWNTs by Ichida *et al.*[17]

Examining the peak shift dependence as a function of population times, the 3PEPS decay profile provides information about spectral diffusion processes in the E_{11} band. The 3PEPS decay profiles shown in Fig. 6(b) were collected under a low excitation fluence of 4.3 μJ/cm^2 at various temperature increments. The room temperature 3PEPS decay profiles have been previously analyzed to obtain spectral lineshapes and estimation of exciton–phonon coupling strengths.[15] Since the low temperature band thermalization processes are not yet well understood in SWNTs, we instead analyze the temperature-dependent 3PEPS profiles qualitatively. Upon cooling, the peak shift decays at a markedly slower rate toward a constant long-time peak shift value of ~22 fs. This long-time offset is largely temperature-independent and suggests a fixed inhomogeneous linewidth contribution arising from static environmental interactions. As the temperature is lowered, the decay rate of the peak shift profile slows considerably [Fig. 6(b)]. This slower 3PEPS decay rate is physically consistent with a smaller thermal phonon population, resulting in a statistically longer time for spectral diffusion to effectively erase the system memory associated with the E_{11} band transition.[35]

In Fig. 6(c), the intensity dependence of the 3EPES profiles is plotted for room temperature data. There is a strong correlation between the excitation fluence dependence of the initial peak shift values and those of the 2PE decay rates extracted in Sec. III C. When normalized to a specified t_{23} time the peak-shift profile measured at various excitation fluences can be approximately superimposed (data not shown).

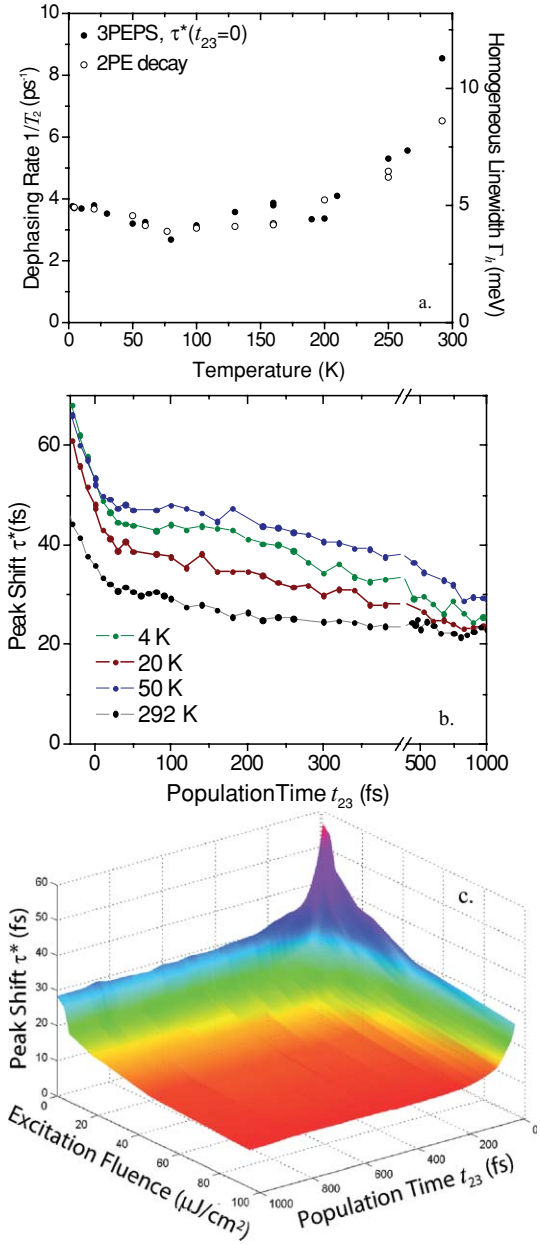

FIG. 6. (a) Comparison of the temperature dependence of the dephasing rate ($1/T_2$) extracted from 2PE experiments and determined from the initial (t_{23} = 0) 3PE peak shift measurements. (b) Temperature dependence of the 3PEPS profile decay. The data was acquired using an SWNT/PVP film at an overall excitation fluence of 4.3 μJ/cm^2. (c) A plot of the photon echo peak shifts acquired at 292 K shown as a function of fluence and population time (t_{23}). The observed intensity dependence at a given population time is qualitatively similar to what is observed from 2PE experiments.

Similar to the 2PE results, we attribute the origin of the intensity-induced spectral diffusion contribution to exciton–exciton scattering processes. Recently, Abramavicius *et al.* modeled this intensity dependence using a nonperturbative phase cycling approach that explicitly accounts for the contribution of exciton–exciton scattering and annihilation processes to the measured photon echo signal. Using this theoretical construct, it was shown that by inclusion of higher than third-order polarization terms, that the observed intensity dependent peak-shift and 2PE profiles can be simulated. The inclusion of higher than third-order terms necessitates the involvement of coherent multiple-exciton states that induce optical dephasing primarily through annihilation pathways.[37] The requirement for multiexciton states to model SWNT photon echo spectroscopy highlights the importance of analyzing photon echo spectroscopy in the regime of low excitation fluence, where such complicating contributions are greatly reduced.

E. Temperature-dependent dephasing and the local environment effect

Below 60 K, the existence of an ~4 nm spectral blueshift in the E_{11} absorption peak of SWNT–PVP polymer composite films [Fig. 1(b) inset], suggests that the possible hydrostatic effects from the local environment may provide an alternative explanation for the acceleration in dephasing rates ($1/T_2$) plotted in Fig. 6(a). To investigate, selected 2PE measurements were repeated with a central excitation wavelength tuned resonantly with the red edge of the E_{11} band at 1012 nm. For a given temperature and excitation fluence, the dephasing times obtained were moderately shorter for excitation at the red edge, but the overall temperature-dependent trend observed (data not shown) was identical to the original resonant excitation case plotted in Fig. 6(a).

Selected for its comparatively small (~2 nm) temperature-dependent E_{11} spectral shift, a gelatin–SWNT composite was used as a model system to investigate how surrounding polymer matrix affects the optical dephasing rates extracted. In Fig. 7(a), the corresponding room temperature dephasing rates are plotted for resonantly excited (6,5) tubes in aqueous solution, PVP polymer, and gelatin composite environments. Our measurements in all three local environments produce long room temperature optical dephasing times (T_2 = 120–205 fs, see Table I).

The temperature-dependent 2PE and 3PEPS measurements previously presented were repeated on resonantly excited (6,5) SWNTs embedded in gelatin composite films. Comparing the 2PE decay profiles obtained for gelatin composites in Fig. 7(b) to PVP polymer composite films shown in Fig. 5(b), the optical dephasing rate is found to have a similar temperature dependence in the two host environments. The corresponding dephasing rates for gelatin composites are plotted in Fig. 7(c) alongside the initial peak shift values. All data presented has been extrapolated to the zero-intensity limit. As with PVP composites, the initial peak shift values measured in gelatin composites show a parallel temperature dependence to the dephasing rates obtained directly from the 2PE decay profile.

The pure dephasing time for gelatin–SWNT composites was determined for select temperatures only. Compared to SWNT aqueous suspensions, moderately faster pure dephasing rates are obtained after incorporating aqueous (6,5) SWNTs into the different polymer environments such as PVP and gelatin. This environmental dependence suggests that the bath fluctuations from the surrounding polymer are moderately coupled to the E_{11} exciton transition; however, under ambient conditions exciton–phonon scattering intrinsic to the SWNT remains the dominant contribution to optical dephasing. As $T \rightarrow 0$, the predicted pure dephasing time for

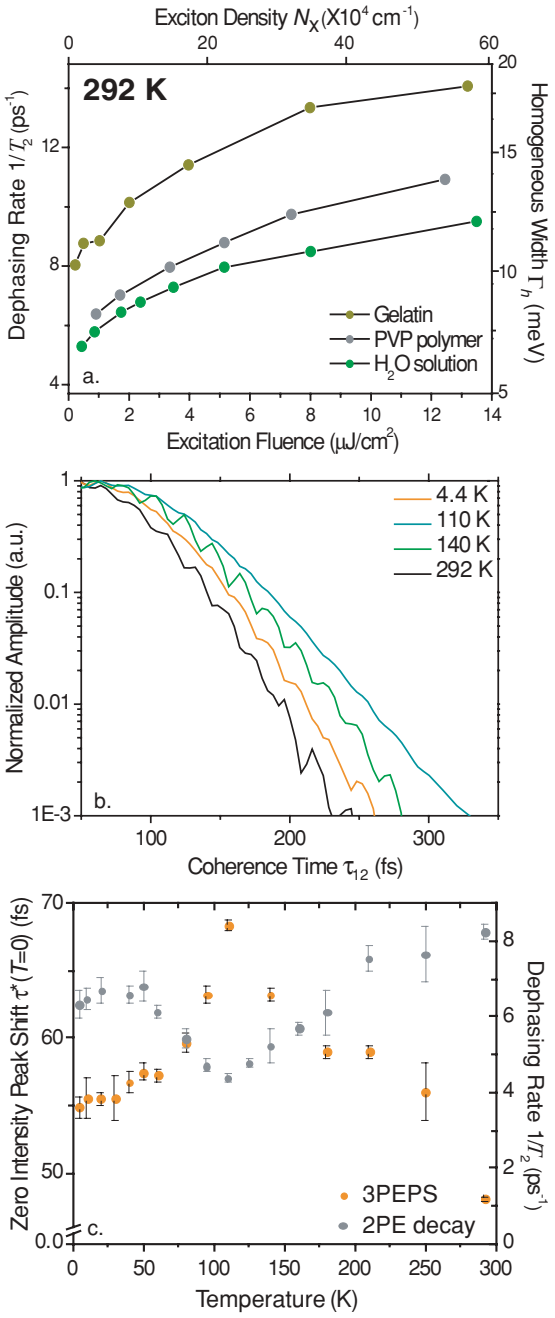

FIG. 7. (a) Extracted room temperature optical dephasing rates for (6,5) SWNTs in different local environments. (b) Temperature-dependent 2PE collected at 6.0 μJ/cm^2 in a gelatin matrix. Below 100 K, T_2 decreases markedly. A weak oscillatory frequency similar to the G-band period is apparent for $T \geq 130$ K. (c) Corresponding peak shift measurements were collected concurrently with 2PE decays for (6,5) SWNTs in gelatin. The peaks shifts were extrapolated to the zero intensity limit, yielding complimentary results.

the gelatin composite is ~30% smaller than the PVP case, suggesting that changes in environmental static disorder and spectral diffusion also contribute substantially to the homogeneous broadening. Effects such as tube proximity and potential tube aggregation after incorporation of SWNTs into polymer environments presents another potential source of disorder requiring further investigation. The timescales of E_{11} exciton dynamics for (6,5) carbon nanotubes are summarized in Table I.

For gelatin–SWNT composites, an oscillatory feature consistent with vibrational beating was also apparent in the 2PE decay during the pulse overlap region. Using singular value decomposition a dominant beat frequency of 1770 cm^{-1} is extracted which is similar to the 1640 cm^{-1} excited-state tangential Raman mode (G-band) for the (6,5) SWNT.[57] Such oscillatory behavior has been previously observed in pump–probe measurements using pulse widths shorter than the G-band vibrational period (~21 fs).[58] Interestingly, for the 2PE measurements this oscillatory component diminishes almost entirely in amplitude for temperatures corresponding to the longest dephasing times. One potential explanation is at low temperature the exciton wavepacket may be sufficiently delocalized to effectively "average over" the coupled G-band tangential mode. This phenomenon of motional narrowing that has been extensively described in other quasi-1D systems such as molecular aggregates.[18,59] If present in SWNTs, motional narrowing may help explain why long pure dephasing times are realized under ambient conditions.

F. Motional narrowing and exciton–phonon coupling strength

Considering the well-defined nanotube vibrational modes, and large surface area exposure to the surrounding environment, the observation of weak exciton–phonon coupling (T_2^* up to 285 fs) at room temperature is perhaps unexpected. Such weak coupling has been previously characterized by the Huang–Rhys parameters giving weakly coupled values of 0.1 and 0.03 for the RBM and G-band modes, respectively.[54] While this study does not provide such phonon specific coupling strengths, we can instead explore the role of motional narrowing in exciton–phonon coupling, by fitting the nonexponential behavior in the 2PE decay profile across a range of temperatures. Using the model discussed below, the shape of 2PE decay profiles suggests the corresponding E_{11} homogeneous linewidths are motionally narrowed for all temperatures measured.

The nonexponential component of the 2PE decay is extracted using a model function derived out of the stochastic Kubo line-shape theory for a system coupled to a fluctuating reservoir of phonons, and full details can be found elsewhere.[19,32,60] In short, an ensemble of E_{11} optical transitions is described by a frequency correlation function ($M(t)$)

TABLE I. Extracted values (in fs) that characterize the various timescales of E_{11} exciton dynamics for (6,5) SWNTs. With the exception of the dephasing time measured at lowest excitation intensity (denoted $T_{2,m}$), all decay times, and peak shifts (τ^*) have been extrapolated to the zero intensity limit.

	T(K)	T_1	T_2	$T_{2,m}$	τ^*	T_2^*
PVP	292	295	162	132	53	223
polymer	80	460	311	275	—	470
	4.4	289	269	242	—	508
Gelatin	292	302	124	121	48	155
	110	683	228	170	68	274
	4.4	146	158	130	55	344
Aqueous	292	372	205	184	52	283

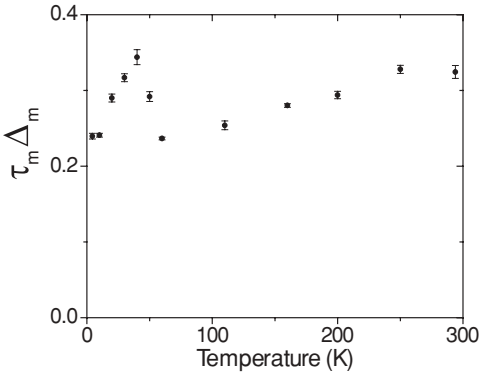

FIG. 8. Modeling the nonexponential component of the decay for the 2PE signal (S_{PE}) for (6,5) SWNTs in PVP polymer permits extraction of the modulation amplitude and time product ($\Delta_m \tau_m \ll 1$) plotted with temperature.

that we assume decays at an exponential rate, $M(t) = e^{-t/\tau_m}$, as the result of exciton coupling to the phonon bath.[32] Here, τ_m is the frequency modulation time that provides the timescale of the phonon frequency perturbations which induce electronic dephasing. The expected profile of a given 2PE curve ($S_E(\tau)$) can then be obtained analytically from $M(t)$,[32]

$$S_E(\tau) = \exp\left\{-4\,(\Delta_m \tau_m)^2 \left[2\exp\left(\frac{-\tau}{\tau_m}\right) - \frac{1}{2}\exp\left(\frac{-2\tau}{\tau_m}\right) + \frac{\tau}{\tau_m} - \frac{3}{2}\right]\right\}, \quad (9)$$

where $\Delta_m \tau_m$ is a dimensionless product of τ_m and the amplitude of the frequency fluctuation (Δ_m). $1/\Delta_m$ represents the minimum time required by the uncertainty principle for an exciton to couple to a phonon mode.[61] If $\tau_m < 1/\Delta_m$, the exciton wavepacket will not couple effectively to the applied fluctuation.[32,61] Hence when $\Delta_m \tau_m \ll 1$, the exciton–phonon coupling process is said to be strongly motionally narrowed. The presence of motional narrowing weakens the effective exciton–phonon coupling strength, resulting in a narrower homogeneous linewidth with a characteristic Lorentzian spectral shape.[18,61]

Across all temperatures investigated, the 2PE decay profile suggests our corresponding homogeneous linewidth is motionally narrowed with an average $\Delta_m \tau_m = 0.28 \pm 0.04$ (see, Fig. 8). Thus, E_{11} excitons in (6,5) SWNTs may not couple effectively to many phonon modes, because nuclear fluctuations from the phonon bath are averaged over from the spatial extent of the exciton along the tube.[18] Certain modes (e.g., the TO optical mode), may couple stronger than others depending upon the geometry and strength the applied nuclear fluctuation. When modes involved in motional narrowing are no longer populated at lower temperature, no net effect on the dephasing time is expected. This observation is in accord with the weak overall temperature dependence associated with the pure optical dephasing rate shown in Fig. 5(b).

In site basis, motional narrowing can be modeled as a form of ballistic exciton transport along the nanotube axis (during T_2^*). This process is fundamentally different from diffusion-limited transport commonly reported on longer timescales observed from intensity-dependent signatures of exciton–exciton annihilation in pump–probe measurements. Ballistic transport implies the exciton is moving faster than it can be thermalized by exciton phonon-coupling. For metallic SWNTs, ballistic transport is a well-established physical property.[62] To check if such a transport process is reasonable for semiconducting SWNTs, we can approximate the kinetic energy of ballistic excitons by $E_{\text{ball}} = 1/2 m^*_{\text{ex}} \left(L_d/T_2^*\right)^2$, where m^*_{ex} is the exciton effective mass and L_d is the exciton delocalization length.[63] In this classical approximation we find $E_{\text{ball}} \approx 3.5 L_d^2 \mu\text{eV/nm}^2$, which exceeds the room temperature thermalization energy (given by $E_k = 1/2 k_b T$) for initial exciton delocalization lengths on the order 50 nm. With literature values for L_d ranging from 10 to 100s of nm,[10,13] this simple classical model suggests the exciton kinetic energy (E_{ball}) may exceed the thermalization energy even at room temperature. Since this model suggests $E_{\text{ball}} > E_k$ for temperatures ranging from 4.4 to 292 K, it is reasonable that E_{11} excitons may experience ballistic transport during the period T_2^*. The presence of ballistic transport further implies that exciton band thermalization may not occur appreciably until after the corresponding T_2^* time has elapsed.[64]

These *ad hoc* calculations for ballistic transport in (6,5) SWNTs, lend support to our 2PE results which suggest a motionally narrowed exciton dephasing process at all temperature measured. As previously reported for quasi-1D molecular aggregates,[18] motional narrowing in SWNTs effectively averages over large dynamic disorder, suggests the presence of considerable exciton delocalization upon optical excitation. This averaging effect reduces the effective exciton–phonon coupling strength and provides a possible explanation for the realization of long 283 fs E_{11} pure optical dephasing times at room temperature.

IV. CONCLUSIONS

We find that motional narrowing is a significant process that modulates the phonon bath fluctuations that couple to the E_{11} exciton state in (6,5) SWNTs. This process effectively weakens the exciton–phonon interaction and helps explain the origin of the unusually long (up to 283 fs) T_2^* times observed at room temperature. Below ~80 K in PVP polymer and ~100 K in gelatin–SWNT composites, a marked increase in dephasing rate was attributed to a corresponding acceleration in the E_{11} population relaxation. Applying a modified three state model previously developed for SWNT PL kinetics,[43] this acceleration in population decay was attributed to exciton thermalization with a low-lying state, found to be ~9 meV below the E_{11} state. By using the dominant population relaxation lifetime (T_1) and the T_2 times extracted from 2PE decay in the low excitation intensity limit, the corresponding pure dephasing times (T_2^*) are calculated. Upon cooling from ambient conditions to 4.4 K, the overall pure dephasing rate decreases just under three fold. Below ~180 K, $1/T_2^*$ decreases linearly consistent with optical dephasing induced by acoustic phonon processes. Such a moderate T_2^* temperature dependence may be expected for ensemble measurements of (6,5) SWNTs because of motional narrowing effects and the presence of a large, environmentally induced

homogeneous linewidth in the low temperature limit. Collectively, this study highlights the important contributions of coherent excitons to the overall E_{11} spectral dynamics of (6,5) SWNTs and suggests an important interplay between exciton–phonon coupling and the exciton delocalization length motivating further investigation.

ACKNOWLEDGMENTS

This work is supported by NSF. The steady-state fluorescence spectra reported in this work were measured at the Molecular Foundry, Lawrence Berkeley National Laboratory, which is supported by the Office of Science, Office of Basic Energy Sciences, of the U.S. Department of Energy under Contract No. DE-AC02-05CH11231. M.W.G. and A.A.G. thank the Natural Sciences and Engineering Research Council of Canada for postgraduate scholarship. Density gradient processing was supported by the National Science Foundation, the Office of Naval Research, and the Nanoelectronics Research Initiative. Y.-Z.M. also acknowledges the support by the Laboratory Directed Research and Development Program of Oak Ridge National Laboratory, managed by UT-Battelle, LLC, for the U.S. Department of Energy. We thank L. V. Valkunas, D. Abramavicius, and Y.-C. Cheng for their helpful contributions.

[1] M. Dresselhaus, G. Dresselhaus, and A. Jorio, Annu. Rev. Mater. Res. **34**, 247 (2004).
[2] Y.-Z. Ma, T. Hertel, Z. V. Vardeny, G. R. Fleming, and L. V. Valkunas, *Ultrafast spectroscopy of carbon nanotubes, Topics in Appl. Phys. Vol. 111* (Springer-Verlag, Berlin, 2008).
[3] K. Welsher, Z. Liu, S. P. Sherlock, J. T. Robinson, Z. Chen, D. Daranciang, and H. Dai, Nat. Nanotechnol. **4**, 773 (2009).
[4] N. Gabor, Z. Zhong, K. Bosnick, J. Park, and P. L. McEuen, Science **325**, 1367 (2009).
[5] F. Wang, G. Dukovic, L. E. Brus, and T. F. Heinz, Science **308**, 838 (2005).
[6] J. Maultzsch, R. Pomraenke, S. Reich, E. Chang, D. Prezzi, A. Ruini, E. Molinari, M. Strano, C. Thomsen, and C. Lienau, Phys. Rev. B **72**, 241402(R) (2005).
[7] Y.-Z. Ma, L. V. Valkunas, S. M. Bachilo, and G. R. Fleming, J. Phys. Chem. B **109**, 15671 (2005).
[8] M. Dresselhaus, G. Dresselhaus, R. Saito, and A. Jorio, Annu. Rev. Phys. Chem. **58**, 719 (2007).
[9] C. D. Spataru, S. Ismail-Beigi, L. Benedict, and S. G. Louie, Phys. Rev. Lett. **92**, 077402 (2004).
[10] V. Perebeinos, J. Tersoff, and P. Avouris, Nano Lett. **5**, 2495 (2005).
[11] J. Shaver and J. Kono, Laser Photonics Rev. **1**, 260 (2007).
[12] J. Shah, *Ultrafast Spectroscopy of Semiconductors and Semiconductor Nanostructures* (Springer-Verlag, Berlin, 1999).
[13] Y. Miyauchi, H. Hirori, K. Matsuda, and Y. Kanemitsu, Phys. Rev. B **80**, 081410 (2009).
[14] T. Joo, Y. Jia, J.-Y. Yu, M. Lang, and G. R. Fleming, J. Chem. Phys. **104**, 6089 (1996).
[15] M. W. Graham, Y.-Z. Ma, and G. R. Fleming, Nano Lett. **8**, 3936 (2008).
[16] Y.-Z. Ma, M. W. Graham, A. A. Green, M. C. Hersam, and G. R. Fleming, Phys. Rev. Lett. **101**, 217402 (2008).
[17] M. Ichida, Y. Kiyohara, S. Saito, Y. Miyata, H. Kataura, and H. Ando, Phys. Status Solidi B **245**, 2712 (2008).
[18] H. Fidder, J. Terpstra, and D. Wiersma, J. Chem. Phys. **94**, 6895 (1991).
[19] S. Mukamel, *Principles of Nonlinear Optical Spectroscopy* (Oxford University Press, New York, 1995).
[20] D.-S. Kim, J. Shah, J. Cunningham, T. Damen, W. Schöfer, M. Hartmann, and S. Schmitt-Rink, Phys. Rev. Lett. **68**, 1006 (1992).
[21] A. Honold, L. Schultheis, J. Kuhl, and C. Tu, Phys. Rev. B **40**, 6442 (1989).
[22] A. Hartschuh, H. Pedrosa, L. Novotny, and T. Krauss, Science **301**, 1354 (2003).
[23] K. Yoshikawa, R. Matsunaga, K. Matsuda, and Y. Kanemitsu, Appl. Phys. Lett. **94**, 093109 (2009).
[24] J. Lefebvre, D. Austing, J. Bond, and P. Finnie, Nano Lett. **6**, 1603 (2006).
[25] M. W. Graham, Y.-Z. Ma, and G. R. Fleming, Proc. SPIE **7600**, 76001F1 (2010).
[26] M. S. Arnold, A. A. Green, J. F. Hulvat, S. I. Stupp, and M. C. Hersam, Nature Nanotechnol. **1**, 60 (2006).
[27] O. Torrens, D. Milkie, M. Zheng, and J. Kikkawa, Nano Lett. **6**, 2864 (2006).
[28] P. Tan, A. Rozhin, T. Hasan, P. Hu, V. Scardaci, W. Milne, and A. Ferrari, Phys. Rev. Lett. **99**, 137402 (2007).
[29] R. B. Capaz, C. D. Spataru, P. Tangney, M. L. Cohen, and S. G. Louie, Phys. Status Solidi B **241**, 3352 (2004).
[30] R. B. Capaz, C. D. Spataru, S. Ismail-Beigi, and S. G. Louie, Phys. Rev. B **74**, 121401(R) (2006).
[31] S. Cronin, Y. Yin, A. Walsh, R. B. Capaz, A. Stolyarov, P. Tangney, M. L. Cohen, S. G. Louie, A. Swan, M. Unlu, B. Goldberg, and M. Tinkham, Phys. Rev. Lett. **96**, 127403 (2006).
[32] M. A. Berg, K. D. Rector, and M. D. Fayer, J. Chem. Phys. **113**, 3233 (2000).
[33] T. Joo and A. Albrecht, Chem. Phys. **176**, 233 (1993).
[34] C. Manzoni, A. Gambetta, E. Menna, M. Meneghetti, G. Lanzani, and G. Cerullo, Phys. Rev. Lett. **94**, 207401 (2005).
[35] M. Cho, J.-Y. Yu, T. Joo, Y. Nagasawa, S. A. Passino, and G. R. Fleming, J. Phys. Chem. **100**, 11944 (1996).
[36] S. Berciaud, L. Cognet, P. Poulin, R. Weisman, and B. Lounis, Nano Lett. **7**, 1203 (2007).
[37] D. Abramavicius, Y.-Z. Ma, M. W. Graham, L. Valkunas, and G. R. Fleming, Phys. Rev. B **79**, 195445 (2009).
[38] K. Matsuda, T. Inoue, Y. Murakami, S. Maruyama, and Y. Kanemitsu, Phys. Rev. B **77**, 033406 (2008).
[39] H. Wagner, W. Langbein, J. Hvam, G. Bacher, T. Kmmell, and A. Forchel, Phys. Rev. B **57**, 1797 (1998).
[40] M. R. Salvador, P. S. Nair, M. Cho, and G. D. Scholes, Chem. Phys. **350**, 56 (2008).
[41] H. van Amerongen, L. Valkunas, and R. van Grondelle, *Photosynthetic Excitons* (World Scientific, Singapore, 2000).
[42] W. Metzger, T. McDonald, C. Engtrakul, J. Blackburn, G. Scholes, G. Rumbles, and M. Heben, J. Phys. Chem. C **111**, 3601 (2007).
[43] G. D. Scholes, S. Tretiak, T. J. McDonald, W. K. Metzger, C. Engtrakul, G. Rumbles, and M. J. Heben, J. Phys. Chem. C **111**, 11139 (2007).
[44] L. V. Valkunas, Y.-Z. Ma, and G. R. Fleming, Phys. Rev. B **73**, 115432 (2006).
[45] C. D. Spataru, S. Ismail-Beigi, R. Capaz, and S. G. Louie, Phys. Rev. Lett. **95**, 247402 (2005).
[46] S. Berger, C. Voisin, G. Cassabois, C. Delalande, P. Roussignol, and X. Marie, Nano Lett. **7**, 398 (2007).
[47] M. Lin and K.-K. Shung, Phys. Rev. B **50**, 17744 (1994).
[48] S. Lin and R. Bersohn, J. Chem. Phys. **48**, 2732 (1968).
[49] R. Matsunaga, Y. Miyauchi, K. Matsuda, and Y. Kanemitsu, Phys. Rev. B **80**, 115436 (2009).
[50] H. Harutyunyan, T. Gokus, A. A. Green, M. C. Hersam, M. Allegrini, and A. Hartschuh, Nano Lett. **9**, 2010 (2009).
[51] K. Matsuda, T. Inoue, Y. Murakami, S. Maruyama, and Y. Kanemitsu, Phys. Rev. B **77**, 193405 (2008).
[52] Y.-Z. Ma, L. V. Valkunas, S. M. Bachilo, and G. R. Fleming, Phys. Chem. Chem. Phys. **8**, 5689 (2006).
[53] A. Hagen, M. Steiner, M. Raschke, C. Lienau, T. Hertel, H. Qian, A. Meixner, and A. Hartschuh, Phys. Rev. Lett. **95**, 197401 (2005).
[54] B. Habenicht, H. Kamisaka, K. Yamashita, and O. Prezhdo, Nano Lett. **7**, 3260 (2007).
[55] R. Saito, C. Fantini, and J. Jiang, *Topics in Applied Physics* (Springer-Verlag, Berlin, Heidelberg, 2008), Vol. 111, pp. 251–285.
[56] A. M. Weiner, S. D. Silvestri, and E. P. Ippen, J. Opt. Soc. Am. B **2**, 654 (1985).

[57]Y.-Z. Ma, M. W. Graham, M. A. Prantil, A. J. Van Tassle, and G. R. Fleming, J. Phys. Chem. B **112**, 16030 (2008).
[58]A. Gambetta, C. Manzoni, E. Menna, M. Meneghetti, G. Cerullo, G. Lanzani, S. Tretiak, A. Piryatinski, A. Saxena, R. Martin, and A. Bishop, Nat. Phys. **2**, 515 (2006).
[59]H. Pschierer and J. Friedrich, Phys. Status Solidi B **189**, 43 (1995).
[60]R. Kubo, Adv. Chem. Phys. **15**, 101 (1969).
[61]Y. Toyozawa, *Optical Processes in Solids* (Cambridge University Press, Cambridge, 2003).
[62]C. T. White and T. N. Todorov, Nature (London) **393**, 240 (1998).
[63]G. Cassabois and R. Ferreira, C. R. Phys. **9**, 830 (2008).
[64]L. Cognet, D. A. Tsyboulski, J.-D. R. Rocha, C. D. Doyle, J. M. Tour, and R. B. Weisman, Science **316**, 1465 (2007).